Appendix for
"FleXOR: Trainable Fractional Quantization"

A Example of a XOR-gate Network Structure Representation

In Figure 2, outputs of an XOR-gate network are given as

$$\begin{aligned}
y_1 &= x_1 \oplus x_3 \oplus x_4 \\
y_2 &= x_1 \oplus x_2 \\
y_3 &= x_1 \oplus x_2 \oplus x_3 \\
y_4 &= x_3 \oplus x_4 \\
y_5 &= x_2 \oplus x_4 \\
y_6 &= x_2 \oplus x_3 \oplus x_4.
\end{aligned}$$

Equivalently, the same structure as above can be represented in a matrix as

$$\boldsymbol{M}^{\oplus} = \begin{bmatrix} 1 & 0 & 1 & 1 \\ 1 & 1 & 0 & 0 \\ 1 & 1 & 1 & 0 \\ 0 & 0 & 1 & 1 \\ 0 & 1 & 0 & 1 \\ 0 & 1 & 1 & 1 \end{bmatrix}. \tag{1}$$

Note that elements of $\boldsymbol{M}^{\oplus}$ are matched with coefficients of $y_i (1 \leq i \leq 6)$. For two vectors $\boldsymbol{y} = \{y_1, y_2, y_3, y_4, y_5, y_6\}$ and $\boldsymbol{x} = \{x_1, x_2, x_3, x_4\}$, the following equation holds:

$$\boldsymbol{y} = \boldsymbol{M}^{\oplus} \cdot \boldsymbol{x}, \tag{2}$$

where element-wise addition and multiplication are performed by 'XOR' and 'AND' function, respectively. In Eq. (1), N_{tap} (i.e., the number of '1's in a row) is 2 or 3.

B Supplementary Data for Basic FleXOR Training Principles

A Boolean XOR gate can be modeled as $\mathcal{F}^{\oplus}(x_1, x_2) = (-1)\,\mathrm{sign}(x_1)\,\mathrm{sign}(x_2)$ if 0 is replaced with -1 as shown in Table 1.

$\mathrm{sign}(x_1)$	$\mathrm{sign}(x_2)$	$\mathcal{F}^{\oplus}(x_1, x_2)$
-1	-1	-1
-1	$+1$	$+1$
$+1$	-1	$+1$
$+1$	$+1$	-1

Table 1: An XOR gate modeling using $\mathcal{F}^{\oplus}(x_1, x_2)$.

In Eq. (1), forward propagation for y_3 is expressed as

$$y_3 = \mathcal{F}^{\oplus}(x_1, x_2, x_3) = (-1)^2\,\mathrm{sign}(x_1)\,\mathrm{sign}(x_2)\,\mathrm{sign}(x_3). \tag{3}$$

34th Conference on Neural Information Processing Systems (NeurIPS 2020), Vancouver, Canada.

while partial derivative of y_3 with respect to x_1 is given as (not derived from Eq. (3))

$$\frac{\partial y_3}{\partial x_1} = S_{\text{tanh}}(-1)^2(1-\tanh^2(x_1 \cdot S_{\text{tanh}}))\tanh(x_2 \cdot S_{\text{tanh}})\tanh(x_3 \cdot S_{\text{tanh}}), \tag{4}$$

or as

$$\frac{\partial y_3}{\partial x_1} \approx S_{\text{tanh}}(-1)^2(1-\tanh^2(x_1 \cdot S_{\text{tanh}}))\,\text{sign}(x_2)\,\text{sign}(x_3). \tag{5}$$

We choose Eq. (5), instead of Eq. (4), as explained in Section 3.

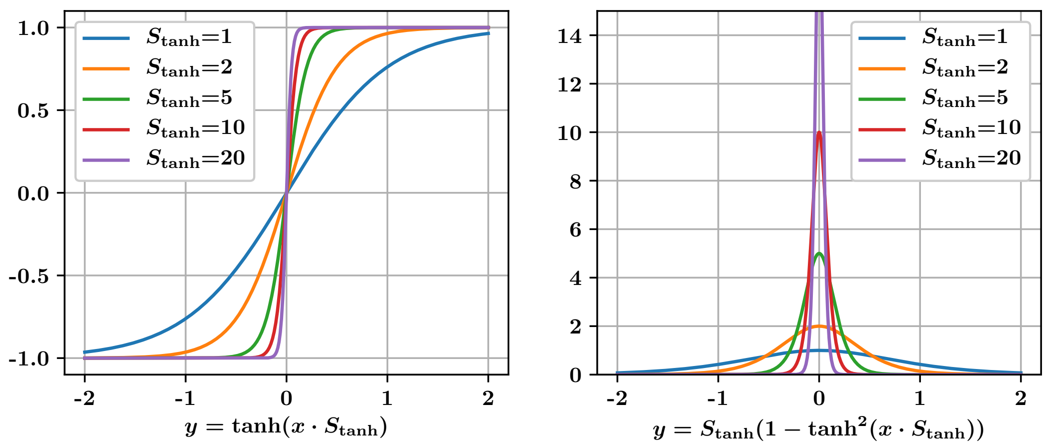

Figure 1: The left graph shows hyperbolic tangent ($y = \tanh(x \cdot S_{\text{tanh}})$) graphs with various scaling factors (S_{tanh}), . The right graph shows their derivatives. These graphs support the arguments of '**Optimize S_{tanh}**' in Section 4.

As shown in Figure 1, large S_{tanh} yields sharp transitions for near-zero inputs. Such a sharp approximation of the Heaviside step function produces large gradient values for small inputs and encourages encrypted weights to be separated into negative or positive values. Too large S_{tanh}, however, has the same issues of a too-large learning rate.

Figure 4 presents training loss and test accuracy when N_{tap}=2 and N_{out} is 10 or 20. Compared with Figure 5, N_{tap}=2 presents improved accuracy for the cases of high compression configurations (e.g., N_{in}=4 and N_{out}=10). We use $N_{tap} = 2$ for CIFAR-10 and ImageNet, since low N_{tap} avoids gradient vanishing problems or high approximation errors in Eq.(5) or Eq.(6).

Figure 5 plots the distribution of encrypted weights at different training steps when each row of $\boldsymbol{M}^{\oplus}$ is randomly assigned with $\{0, 1\}$ (i.e., N_{tap} is $N_{in}/2$ on average) or assigned with only two 1's (N_{tap}=2). Due to gradient calculations based on tanh and high S_{tanh}, encrypted weights tend to be clustered on the left or right (near-zero encrypted weights become less as N_{tap} increases) even without weight clipping.

C Supplementary Experimental Results of CIFAR-10 and ImageNet

In this section, we additionally provide various graphs and accuracy tables for ResNet models on CIFAR10 and ImageNet. We also present experimental results from wider hyper-parameters searches including q=2 with two separate $\boldsymbol{M}^{\oplus}$ configurations (with the same N_{in} and N_{out} for two $\boldsymbol{M}^{\oplus}$ matrices).

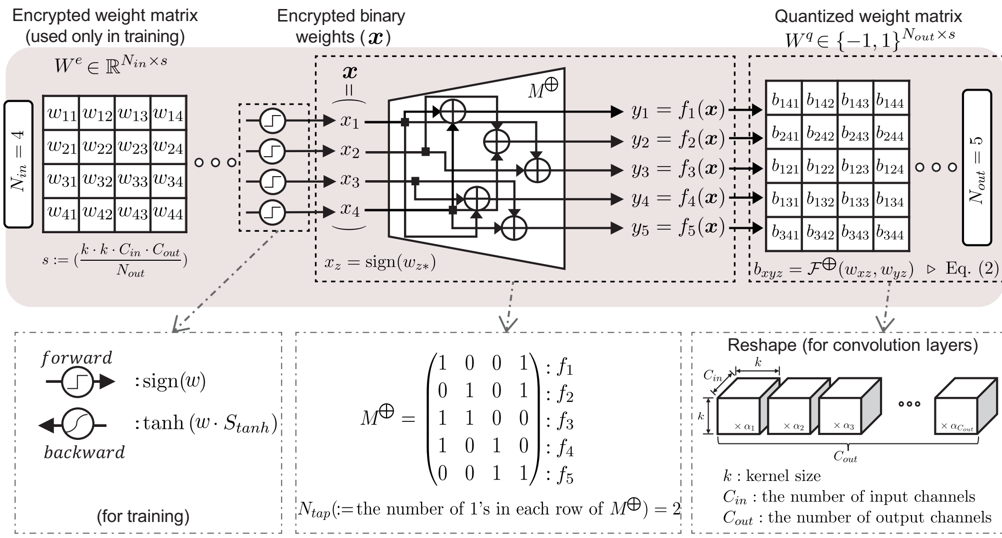

Figure 2: An example showing FleXOR operations for training. XOR gates are described in different ways for forward- and backward propagation. Once we obtain encrypted binary weights after training, we use digital XOR gates for inference.

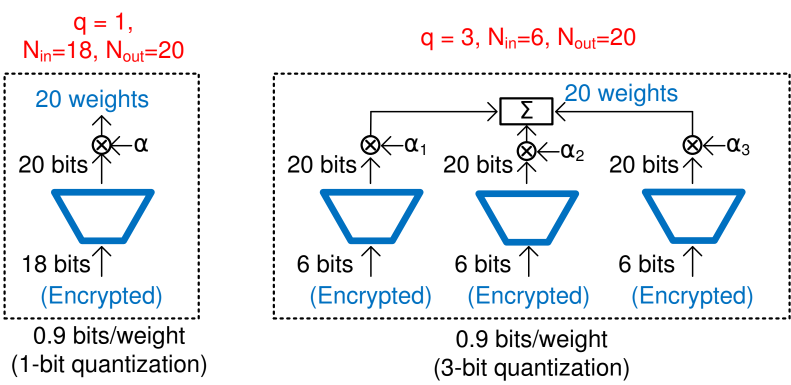

Figure 3: Using the same weight storage footprint, FleXOR enables various internal quantization schemes. (Left): 1-bit internal quantization. (Right): 3-bit internal quantization with 3 different $\boldsymbol{M}^{\oplus}$ configurations.

	Bits/Weight	ResNet-20		ResNet-32		Comp. Ratio
FP	32	91.87%	Diff.	92.33%	Diff.	1.0x
N_{in}=10, N_{out}=10	1.0	90.21%	-1.66	91.40%	-0.93	29.95×
N_{in}=9, N_{out}=10	0.9	90.03%	-1.84	91.28%	-1.05	31.82×
N_{in}=8, N_{out}=10	0.8	89.73%	-2.14	90.96%	-1.37	35.32×
N_{in}=7, N_{out}=10	0.7	89.88%	-1.99	90.67%	-1.66	39.68×
N_{in}=6, N_{out}=10	0.6	89.21%	-2.66	90.41%	-1.92	45.27×
N_{in}=5, N_{out}=10	0.5	88.59%	-3.28	89.95%	-2.38	52.70×

Table 2: Weight compression comparison of ResNet-20 and ResNet-32 on CIFAR-10 when N_{out}=10. Parameters and recipes not described in the table are the same as in Table 1. We also present compression ratio for fractional quantized ResNet-32 when one scaling factor (α) is assigned to each output channel.

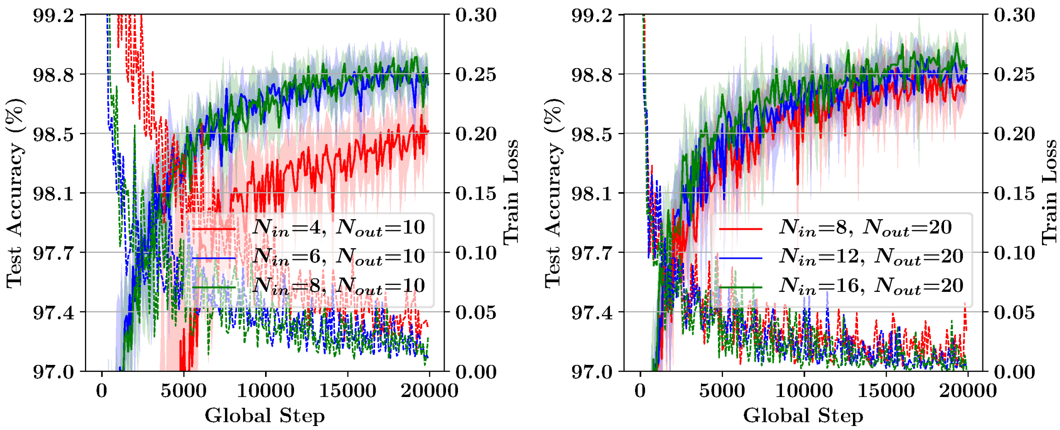

Figure 4: Test accuracy and training loss of LeNet-5 on MNIST when number of '1's in each row of $\boldsymbol{M}^{\oplus}$ is fixed to be 2 (N_{tap}=2). N_{out} is 10 or 20 to generate, effectively, 0.4, 0.6, or 0.8 bit/weight quantization. With low N_{tap} of $\boldsymbol{M}^{\oplus}$, MNIST training presents less variations on training loss and test accuracy that in Figure 5.

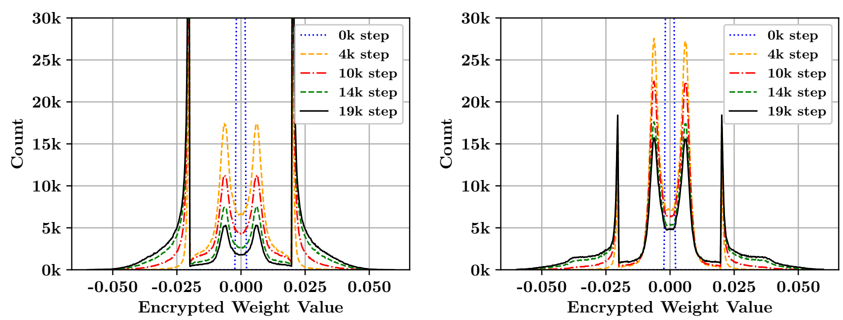

Figure 5: Distribution of encrypted weight values for FC1 layer of LeNet-5 at different training steps using $S_{\tanh}$=100 and N_{out}=10. (Left): $\boldsymbol{M}^{\oplus}$ is randomly filled ($N_{tap} \approx N_{in}/2$). (Right): $N_{tap} = 2$ for every row of $\boldsymbol{M}^{\oplus}$.

	ResNet-20			ResNet-32		
	FP	Quant.	Diff.	FP	Quant.	Diff.
TWN (ternary)	92.68%	88.65%	-4.03	93.40%	90.94%	-2.46
BinaryRelax (ternary)	92.68%	90.07%	-1.91	93.40%	92.04%	-1.36
TTQ (ternary)	91.77%	91.13%	-0.64	92.33%	92.37%	+0.04
LQ-Net (2 bit)	92.10%	91.80%	-0.30	-	-	-
FleXOR($q=2$, $N_{out}=20$)						
N_{in}=20, 2.0 bit/weight		91.38%	-0.49		92.25%	-0.08
N_{in}=18, 1.8 bit/weight		91.00%	-0.87		92.27%	-0.06
N_{in}=16, 1.6 bit/weight	91.87%	90.88%	-0.99	92.33%	92.11%	-0.22
N_{in}=14, 1.4 bit/weight		90.90%	-0.97		92.02%	-0.31
N_{in}=12, 1.2 bit/weight		90.56%	-1.31		91.62%	-0.71
FleXOR($q=2$, $N_{out}=10$)						
N_{in}=10, 2.0 bit/weight		91.19%	-0.68		92.61%	+0.28
N_{in}=9, 1.8 bit/weight		91.44%	-0.43		92.09%	-0.24
N_{in}=8, 1.6 bit/weight	91.87%	91.10%	-0.77	92.33%	92.08%	-0.25
N_{in}=7, 1.4 bit/weight		90.94%	-0.93		91.74%	-0.59
N_{in}=6, 1.2 bit/weight		90.56%	-1.31		91.37%	-0.96

Table 3: Weight compression comparison of ResNet-20 and ResNet-32 on CIFAR-10 using learning rate warmup (for 100 epochs) and q=2. As mentioned in Figure 6, multiple $\boldsymbol{M}^{\oplus}$ can be combined for multi-bit quantization schemes. Then, the number of scaling factors should be doubled. FleXOR with q=2 and two different $\boldsymbol{M}^{\oplus}$ structures achieve full-precision accuracy when both N_{in} and N_{out} are 10.

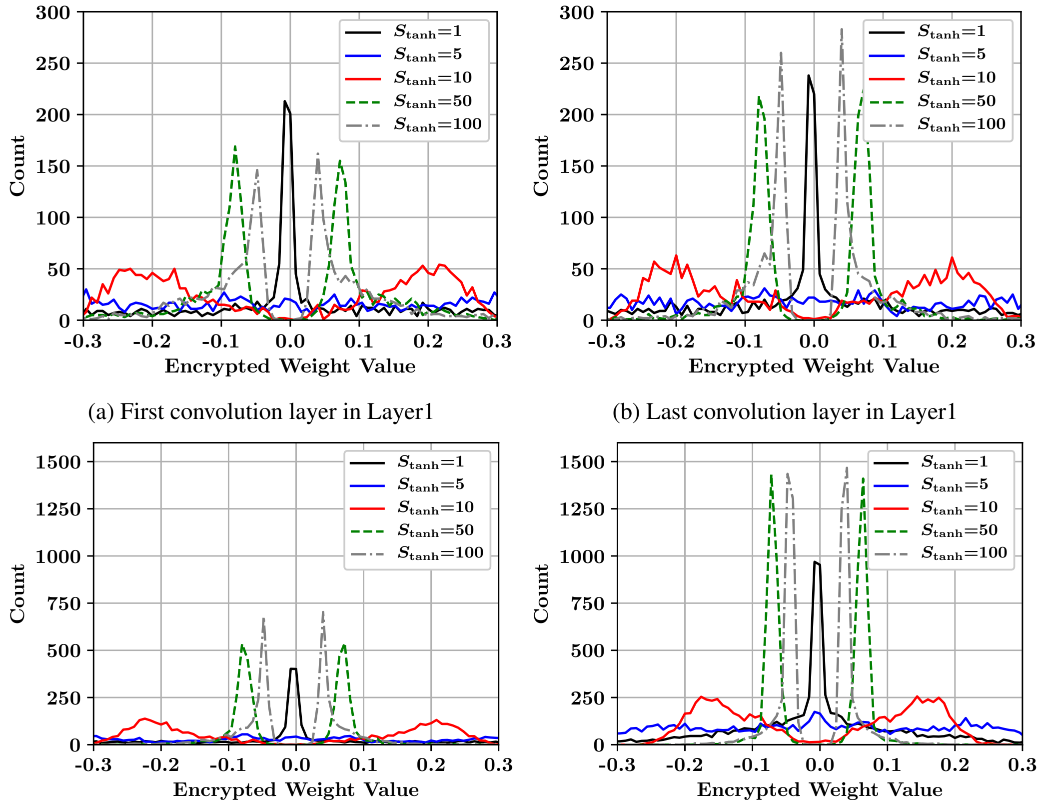

(a) First convolution layer in Layer1

(b) Last convolution layer in Layer1

(c) First convolution layer in Layer2

(d) Last convolution layer in Layer2

Figure 6: Distributions of encrypted weights (at the end of training) in various layers of ResNet-32 on CIFAR-10 using various S_{tanh} and the same N_{out}, N_{in}, and q as Figure 7. The ResNet-32 network mainly consists of three layers according to the feature map sizes: Layer1, Layer2 and Layer3.

Methods	Bits/Weight	Top-1	Top-5
Full Precision [1]	32	69.6%	89.2%
TWN [3]	ternary	61.8%	84.2%
ABC-Net [4]	2	63.7%	85.2%
BinaryRelax [5]	ternary	66.5%	87.3%
TTQ(1.5× Wide) [7]	ternary	66.6%	87.2%
LQ-net [6]	2	68.0%	88.0%
QIL [2]	2	68.1%	88.3%
FleXOR (q=2, N_{out}=20)	1.6 (0.8×2)	66.2%	86.7%
	1.2 (0.6×2)	65.4%	86.0%
	0.8 (0.4×2)	63.8%	85.0%

Table 4: Weight compression comparison of ResNet-18 on ImageNet when q=2. Since q is 2, we also list the other compression schemes which use 2-bit or ternary quantization scheme for model compression.

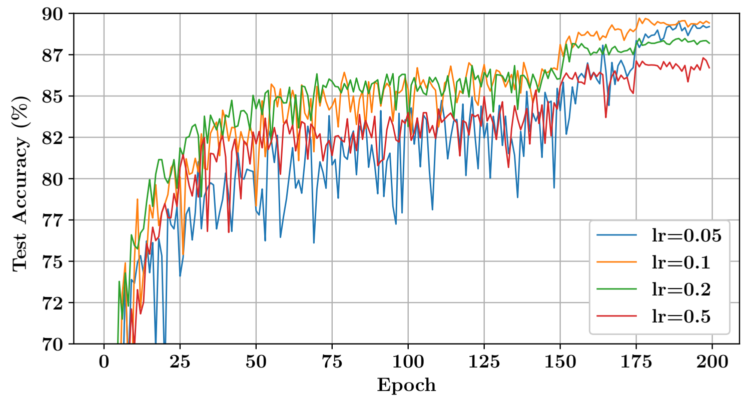

(a) **Initial Learning Rate (0.1)**: Test accuracy of ResNet-32 on CIFAR10 using the learning schedule in Figure 7 and various initial learning rates (0.05, 0.1, 0.2, 0.5).

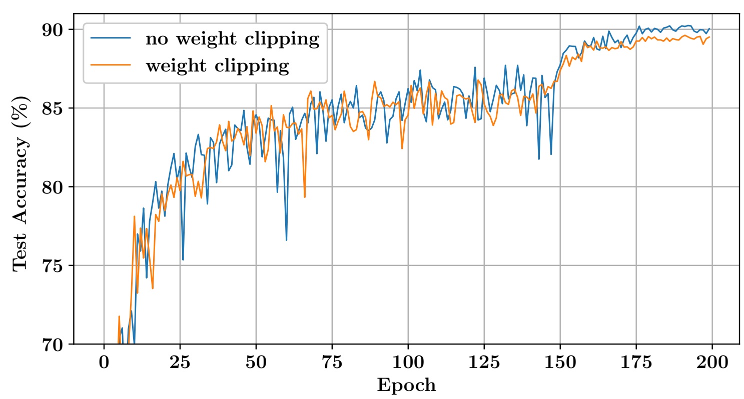

(b) **No Weight Clipping**: Test accuracy of ResNet-32 on CIFAR10 using the learning schedule in Figure 7. As for weight clipping, we restrict the encrypted weights to be ranged as $(-2.0/S_{\tanh}, +2.0/S_{\tanh})$. As can be observed, the red line implies that weight clipping is not effective with FleXOR.

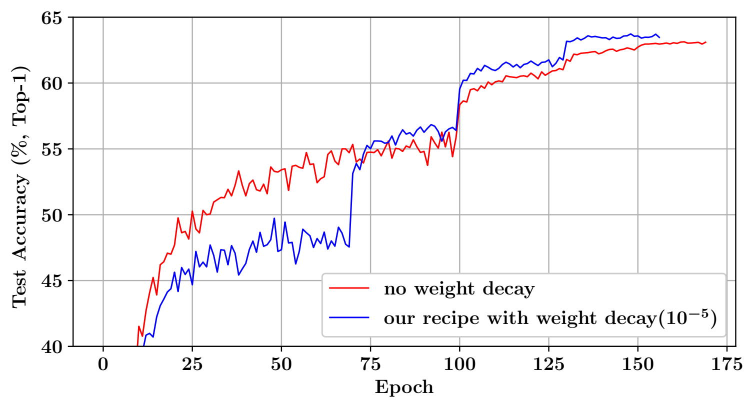

(c) **Weight Decay Factor (10^{-5})**: Two graphs depict test accuracy of ResNet-18 on ImageNet with or without weight decay. The learning rate in the red line (no weight decay) is reduced by half at the 100^{th}, 130^{th} and 150^{th} epochs. The learning rate of the blue line (with weight decay) is reduced by half at 70^{th}, 100^{th} and 130^{th} epochs. With weight decay (blue graph), despite slow convergence in the early training steps, model accuracy is eventually higher than the red one without weight decay scheme.

Figure 7: Comparison of various hyper-parameter choices for CIFAR-10 or ImageNet.

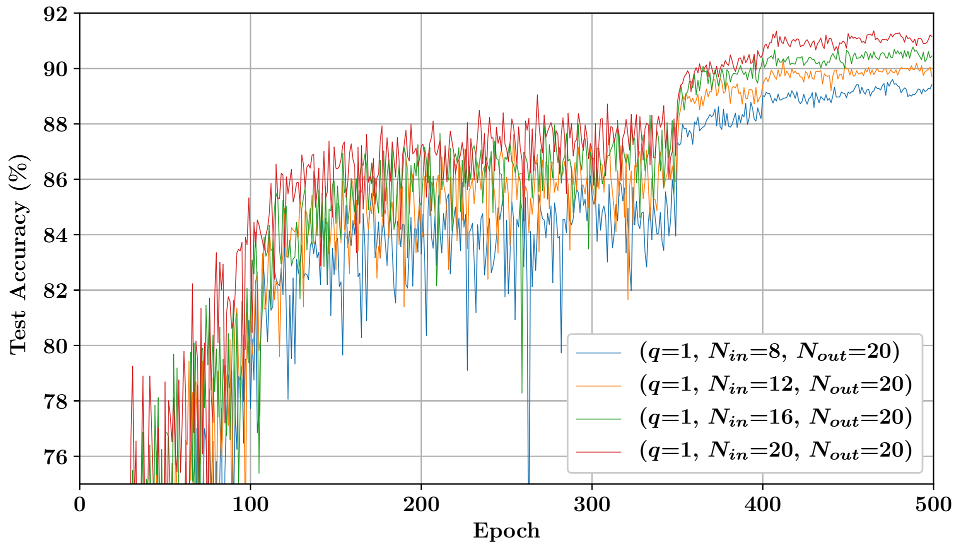

(a) Test accuracy using q=1.

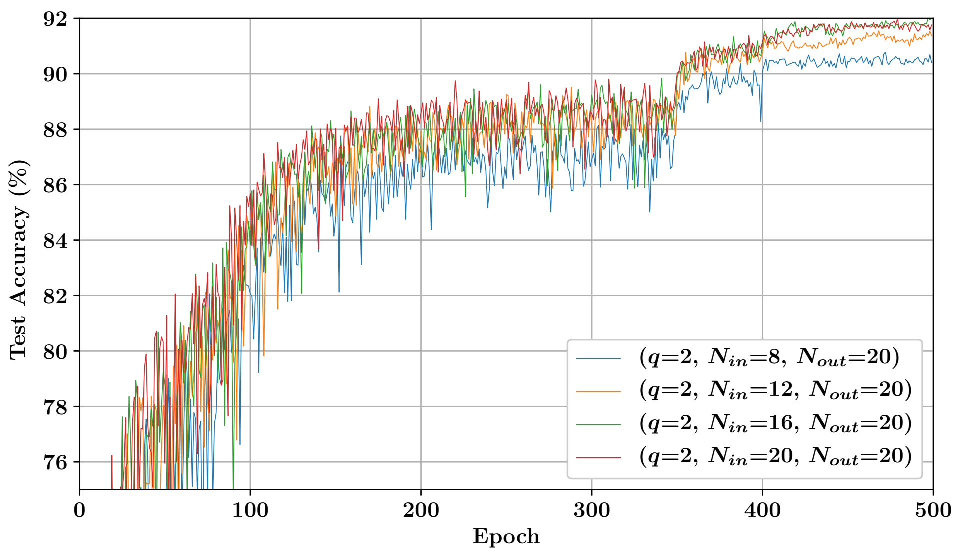

(b) Test accuracy using q=2. Compared to the above plots (Figure 8a), this figure shows that a combination of multiple $\boldsymbol{M}^{\oplus}$ for a binary code can lead to stable learning curves and higher model accuracy.

Figure 8: Test accuracy of ResNet-32 on CIFAR-10 using learning rate warmup (for 100 epochs) and N_{out}=20

References

[1] K. He, X. Zhang, S. Ren, and J. Sun. Deep residual learning for image recognition. *2016 IEEE Conference on Computer Vision and Pattern Recognition (CVPR)*, pages 770–778, 2016.

[2] S. Jung, C. Son, S. Lee, J. Son, J.-J. Han, Y. Kwak, S. J. Hwang, and C. Choi. Learning to quantize deep networks by optimizing quantization intervals with task loss. In *Proceedings of the IEEE Conference on Computer Vision and Pattern Recognition*, pages 4350–4359, 2019.

[3] F. Li and B. Liu. Ternary weight networks. *arXiv:1605.04711*, 2016.

[4] X. Lin, C. Zhao, and W. Pan. Towards accurate binary convolutional neural network. In *Advances in Neural Information Processing Systems*, pages 345–353, 2017.

[5] P. Yin, S. Zhang, J. Lyu, S. Osher, Y. Qi, and J. Xin. Binaryrelax: A relaxation approach for training deep neural networks with quantized weights. *SIAM Journal on Imaging Sciences*, 11 (4):2205–2223, 2018.

[6] D. Zhang, J. Yang, D. Ye, and G. Hua. Lq-nets: Learned quantization for highly accurate and compact deep neural networks. In *Proceedings of the European Conference on Computer Vision (ECCV)*, pages 365–382, 2018.

[7] C. Zhu, S. Han, H. Mao, and W. J. Dally. Trained ternary quantization. In *International Conference on Learning Representations (ICLR)*, 2017.